

An analogue contact probe using a compact 3D optical sensor for micro/nano coordinate measuring machines

This content has been downloaded from IOPscience. Please scroll down to see the full text.

2014 Meas. Sci. Technol. 25 094008

(<http://iopscience.iop.org/0957-0233/25/9/094008>)

View [the table of contents for this issue](#), or go to the [journal homepage](#) for more

Download details:

IP Address: 140.112.43.183

This content was downloaded on 07/11/2014 at 07:49

Please note that [terms and conditions apply](#).

An analogue contact probe using a compact 3D optical sensor for micro/nano coordinate measuring machines

Rui-Jun Li¹, Kuang-Chao Fan^{1,2}, Jin-Wei Miao¹, Qiang-Xian Huang¹, Sheng Tao¹ and Er-min Gong¹

¹ School of Instrument Science and Opto-electronic Engineering, Hefei University of Technology, Tunxi Road 193, Heifei 230009, People's Republic of China

² Department of Mechanical Engineering, National Taiwan University, 1, Sec. 4, Roosevelt Road, Taipei, 10617 Taiwan

E-mail: RJ-Li@hfut.edu.cn

Received 26 January 2014, revised 2 June 2014

Accepted for publication 5 June 2014

Published 12 August 2014

Abstract

This paper presents a new analogue contact probe based on a compact 3D optical sensor with high precision. The sensor comprises an autocollimator and a polarizing Michelson interferometer, which can detect two angles and one displacement of the plane mirror at the same time. In this probe system, a tungsten stylus with a ruby tip-ball is attached to a floating plate, which is supported by four V-shape leaf springs fixed to the outer case. When a contact force is applied to the tip, the leaf springs will experience elastic deformation and the plane mirror mounted on the floating plate will be displaced. The force–motion characteristics of this probe were investigated and optimum parameters were obtained with the constraint of allowable physical size of the probe. Simulation results show that the probe is uniform in 3D and its contacting force gradient is within $1 \text{ mN} \mu\text{m}^{-1}$. Experimental results indicate that the probe has 1 nm resolution, $\pm 10 \mu\text{m}$ measuring range in $X-Y$ plane, $10 \mu\text{m}$ measuring range in Z direction and within 30 nm measuring standard deviation. The feasibility of the probe has been preliminarily verified by testing the flatness and step height of high precision gauge blocks.

Keywords: analogue probe, optical sensor, stiffness, micro/nano-coordinate measurement machine

(Some figures may appear in colour only in the online journal)

1. Introduction

Higher demands on accuracy and precision for measurements of micro and nanostructures over large ranges arise from the microelectronics, optics and precision engineering industries. During the past decade, different micro/nano-coordinate measuring machines (CMMs) that can realize full three-dimensional measurements of increasingly smaller and complex structures have been developed. Most of them are equipped with a contact probe to measure the geometrical dimensions, such as line, plane, circle, sphere, cone, etc [1–5]. A variety of contact probe systems have been designed with different structures and sensors for micro/nano-CMMs. The different micro/nano-CMM probe heads can be classified by

their type of probing system. The first type is the capacitive probe. Capacitive sensors have been used in probes because of their high resolution [6–8]; however, capacitive sensors generally suffer from non-linearity, limited range and drift. The second type is the deformation sensing probe by strain gauges [2, 9–12]. The deformation of the membrane or cantilever caused by the tip ball's motion is detected by the strain gauges, usually made by semiconductor patterning techniques, based on the piezo-resistive effect. These probes can reach 1 nm resolution and have high precision. Nevertheless, the membrane or cantilever is fragile since it does not tolerate large deformations and the probe's displacement range is limited. The third one is the touch-scanning probe based on inductive sensors [13]. A parallel kinematic structure of flexure hinges

is used to minimize the moving mass and ensure an isotropic low stiffness. The probe has a stiffness of 20 mNmm^{-1} , repeatability is claimed to be 5 nm . The fourth kind is the fiber probe with position detectors [14–16] or Bragg grating [17–19]. The former has an especially long probe shaft and especially low contact force, but the precision is not in the nanometer range because the probing system uses illumination of the probe and video to detect the sphere position. The latter is only sensitive to the axial direction of the fiber stem. The fifth kind is the optical sensing probe employing various optical principles, such as triangulation [20], focusing [21, 22], interferometer [23–25] and laser trapping [26]. These probes are usually composed of a stylus, a suspension system and optical sensors to detect the angle or displacement of the probe. Although optical sensors have high resolution and accuracy, however, they have large contact surfaces (spot diameter of about $1\mu\text{m}$ or more) and have trouble in measuring tilted surfaces with high slopes. The sixth kind is a vibrating probe [27–29]. The contact force of vibrating probes is much lower than that of optical sensors, but can only be used as a trigger probe. Weckenmann reviewed some other probe systems published before 2004 [30], and the aspects that influence the interaction between a probe tip and a workpiece during tactile probing are discussed by Bos [31].

In practice, the probe has to meet some basic requirements for detecting complex structures, such as nano-resolution and precision, micrometer measuring range, allowing only elastic deformation, uniform stiffness, high natural frequency and compact size. However, every existing probe shows particular advantages and disadvantages. For instance, most probes are only of touch-trigger type or only possess a few micrometers scanning range.

The authors' group has developed two scanning tactile probes before [21, 32, 33], both of which were based on a monolithic fiber stylus and a wire-suspended floating plate mechanism, but with different sensors. One used four focus sensors and the other was improved with a developed miniature Michelson interferometer and a 2D angle sensor modified from a DVD pickup head. However, it was found in practice that the tensions of the wires were difficult to adjust evenly due to lack of tensile sensor. In addition, the linearity of the wire deformation was not long enough.

This paper presents the development of a new practicable analogue contact probe comprising a compact 3D optical sensor, a tungsten stylus with a ruby tip-ball and four V-shaped leaf springs mechanism to obtain large probe deflection and high precision. The measuring standard deviations are all within 30 nm in the measuring range of $\pm 10\mu\text{m}$ in X – Y plane and $10\mu\text{m}$ in Z direction. The probe has been designed, simulated, fabricated, assembled and calibrated. Some experiments and measurement examples are also conducted.

2. The probe's design

The developed analogue contact probe is composed of a tungsten stylus with a ruby tip-ball, an elastic mechanism consisting of a floating plate and four V-shaped leaf springs, a plane mirror and

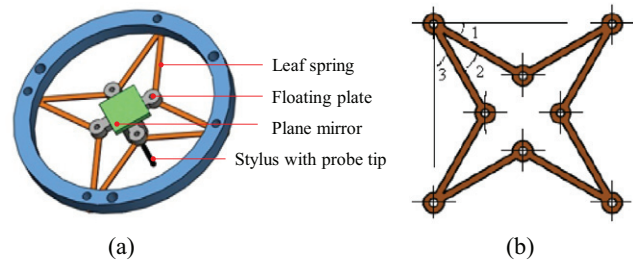


Figure 1. The design of the probe, (a) the probe system, (b) the monolithic spring plate.

a 3D optical sensor. Figure 1(a) shows the probe mechanism. The idea of proposing such an innovative V-shaped four-leaf spring structure is to permit larger tip-ball motion and uniform stiffness in the XY -plane. Although it is over constrained, its symmetrical joints (90° separation) can be more precisely positioned in fabrication comparing with common three-leg design of 120° separation [6]. Figure 1(b) shows the design of the spring, which is made by wire cut on a thin copper plate. The V-angle is 30° and is equivalent to two side angles (1 and 3). Computer simulation in the next section will prove the applicability of this probe. The stylus is screwed into the floating plate to allow easy changeability. When a contact force is applied to the stylus tip-ball, due to elastic deformation of each spring, the floating plate will be tilted and displaced. The vertical displacement and the dual-axis tilts of the plate are detected by the 3D optical sensor with respect to the mirror mounted on the center of the floating plate. With such a configuration the movement of the probe tip, due to the contact force, in X , Y and Z directions can be solved by the three sensing signals (θ , φ and Z).

2.1. Theoretical analysis of elastic mechanism

The main task of the floating plate is to assure the probe a stable rest position when a contact force is applied in three orthogonal directions. The dimensions of the floating plate, as well as the leaf springs, are to be determined according to the required tip-ball movement and contact forces. The permissible overall size of the probe is the constrained condition. Due to its symmetrical geometry, the force–motion characteristics will be automatically symmetrical in the X – Y plane. In order to analyze the response of the displacement to the contact force, the mechanical structure shown in figure 2 is taken into account. Figure 3 illustrates the free body diagram of the floating plate. Compared with the leaf spring, the elastic deformation of the floating plate is relatively smaller. The floating plate is treated as a rigid body in the analysis. The stiffnesses of the probe in vertical (K_v) and horizontal (K_h) directions can be analyzed with the theory of elasticity [34].

$$K_v = \frac{F_{b,v}}{\delta_{b,v}} = \frac{96EI}{L^3} \tag{1}$$

$$K_h = F_h / \delta_{b,h} = \frac{4}{L^3 l^2} [GJL^2 + 2EI(6r^2 + 3r \sin\beta + 3r L \sin\beta + L) + 2EI(6a^2 + 3a \cos\beta + 3aL \cos\beta + L)] \tag{2}$$

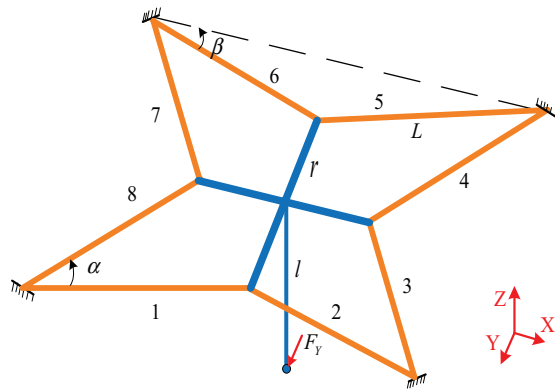


Figure 2. Simplified structure of the probe mechanism.

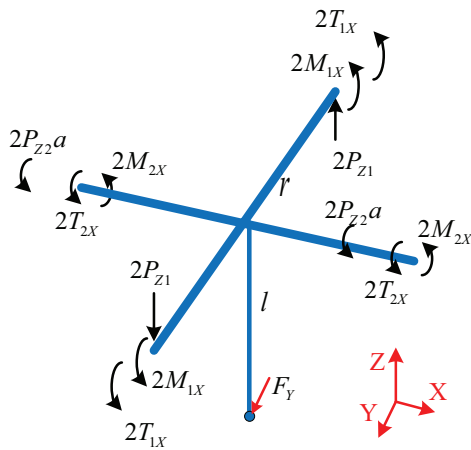


Figure 3. Free body diagram of the floating plate.

where $I = \frac{1}{12}wt^3$, $J = \frac{1}{16}wt^3(\frac{16}{3} - 3.36t/w)$, $G = E/[2(1 + \nu)]$, and β is the angle between leaf spring 6 and the X direction as shown in figure 1(b).

The parameters affecting the stiffness are the leaf spring's dimensions (length L , thickness t and width w), the leaf spring's Poisson ratio ν , the stylus length l , the arm length r , one-half of the arm width a and the Young's modulus of the wire material E .

The probe should be isotropic in all directions and should have low stiffness. The magnitude of the probing force between the tip-ball and the workpiece must be less than the yield stress of the tip ball, stylus and the workpiece to ensure that plastic deformation does not take place. The limit of the probe's stiffness depends on the probe size, probe material and the workpiece material. The maximum admissible force for a 0.3 mm diameter ruby sphere probing on alloy steel is approximately 11.9 mN, according to the Hertz theory [22]. Considering that the targeted range of this probe is $\pm 10 \mu\text{m}$ in 3D, the stiffness of this probe should be less than $1 \text{ mN}/\mu\text{m}^{-1}$. If a 0.5 mm diameter ruby sphere is chosen, the safety factor will be larger. The optimum parameters are calculated by the optimization method, as given in table 1.

The stiffness in Z direction $K_z (= F_z/\delta_{b,z})$ is obtained as 0.943 Nmm^{-1} according to equation (1). In order to find uniform stiffness in vertical and horizontal directions, the stylus length (l) is the most convenient one to be adjusted. Let equation (1) be equal to equation (2), the value of l can

Table 1. The components of the probe mechanism.

Item	Specifications
Leaf springs	Material: beryllium–copper alloy, $E = 130 \times 10^9 \text{ Pa}$, thickness: 0.1 mm, width: 2 mm, length: $L = 13 \text{ mm}$
Floating plate	Material: aluminum alloy, $E = 7.1 \times 10^{10} \text{ Pa}$, thickness: 1.5 mm, arm length: $r = 5.5 \text{ mm}$, arm width: 2 mm; weight: 1.3 g
Stylus	Material: tungsten stylus with a ruby ball tip, $E = 1.93 \times 10^{11} \text{ Pa}$, length: $l = 10 \text{ mm}$, diameter 0.5 mm; weight: 1.2 g

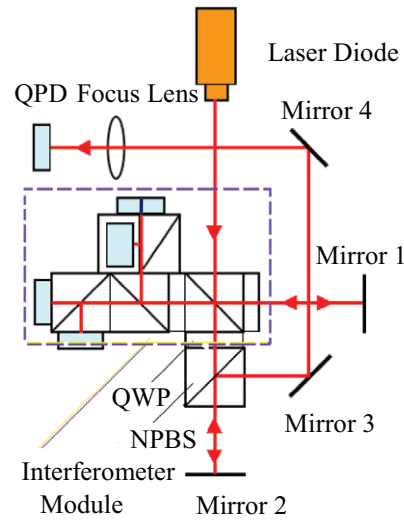


Figure 4. Sketch of the 3D optical sensor.

be obtained as 9.6 mm. Then, K_y and K_x will be the same as K_z ($= 0.943 \text{ Nmm}^{-1}$).

2.2. The 3D optical sensor

The motion of the floating plate is detected by the 3D optical sensor that comprises a miniaturized polarizing interferometer [33, 35] and a micro autocollimator, as shown in figure 4. The optical system of the sensor only utilizes a single laser diode. Therefore, only one plane mirror is mounted on the floating plate. The reflected beam from mirror 2 is split by a non-polarizing beam splitter (NPBS). One part of the beam enters a quadrant photodiode (QPD) to detect the tilt of the floating plate about the horizontal axes based on the autocollimation principle. The other part is fed back into the interferometer module to determine the tip's motion along the vertical axis based on the Michelson interferometer principle. Therefore, with this integral sensor it is possible to simultaneously measure the tip's displacement along the three axes.

Because a polarizing beam splitter (PBS) and two quarter wave plates (QWP) are adopted in the interferometer module, the reflected beam does not go back to the laser diode to disturb its intensity. The advantages of this sensor include: (1) the structure is simple and the probe's dimension is small, (2) fewer optical components are needed, (3) easy assembly, (4) loss of intensity and parasitic interference on the quadrant photodiode are avoided, and (5) both the autocollimator and the interferometer are sensitive to the 3D motions of the



Figure 5. Photo of the probe.

mirror 2 (θ , φ and Z). The only disadvantage is that the horizontal range is limited because the reflected beam will gradually depart from the reference beam in the interferometer when probing in the horizontal direction. However, experimental results have proved that the permissible horizontal range could reach more than $\pm 10\mu\text{m}$, which is large enough for an analogue probe.

The mechanical structures of the probe head have been optimized so as to obtain a smaller outer dimension. A photo of the 3D microprobe system is shown in figure 5.

The accuracy of the 3D optical sensor has been calibrated by experiments with reference to the Renishaw interferometer (XL80). The miniature polarizing interferometer and the XL80 measured the same displacement generated by a high precision linear stage from opposite sides at the same time. The rays of the two lasers should be coincident in space, so as to eliminate the Abbe error and the cosine error. The measurement procedures were repeated five times over a $20\mu\text{m}$ range and the standard deviation was found to be about 6.3 nm. The non-linearity error was 11 nm. Similarly, the miniature autocollimator and the XL80 synchronously detected the rotational angle of the mirror actuated by a high precision automated turntable. The measurement range of the autocollimator was ± 400 arcsec. Nine points with equal intervals were measured over the whole measurement range, five measurements were repeated and the standard deviation was calculated at every point. The maximum standard deviation of nine points was less than 0.21 arcsec. The corresponding lateral displacement of the tip-ball is about 11.3 nm when the length of the stylus is 11 mm. Therefore, the 3D optical sensor is sensitive enough to be used as a probe.

3. Simulation of the contact force and vibration modes

3.1. Contact force

In order to validate the correctness of the stiffness model, computer simulation is also carried out by finite element method using ANSYS V12 software. The parameters shown

in table 1 are considered. The tip's displacements when a 1 mN force is applied in vertical and in horizontal directions are shown in figures 6(a) and (b), respectively. The resulting tip displacement of $1.08\mu\text{m}$ is the same in both directions. From figure 6(b), we can also see that the rotation point is at the center of the structure and the lateral displacement of the mirror in X - Y is only a few nanometers when applying 1 mN horizontal force. Figure 6(c) shows the tip's uniform displacements when a 1 mN force is applied in different horizontal directions. The tip moves $1.08\mu\text{m}$ in all directions corresponding to a uniform stiffness of 0.926N mm^{-1} . The simulated results are quite consistent with the analytical results and the difference is less than 1.8%.

3.2. Vibration modes

The tip-ball will obtain a little kinetic energy and bounce on the surface of the specimen when in contact with the specimen at a certain speed. The bounce action will not stop before the kinetic energy is depleted. The more kinetic energy the ball tip obtains, the larger its bouncing amplitude will be. Therefore, a higher natural frequency is essential for the probe. In addition, a higher frequency is also beneficial to the measurement speed and resists the lower frequency of the environment.

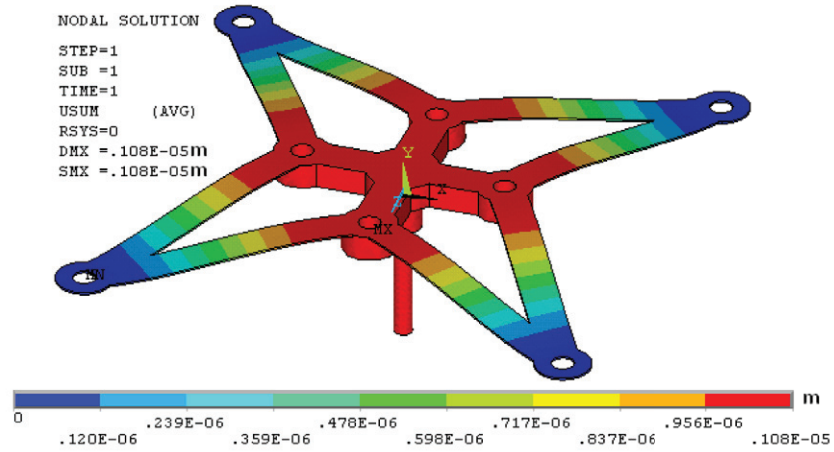
The kinetic energy of the tip-ball obtained during contact with the specimen will transfer to the elastic potential energy of the tip-ball and the specimen. The bouncing times depend on the amount of kinetic energy and the depleted elastic potential energy at every bounce. For our probe, the weight of the stylus and the floating plate is about 2.5 g. When the measurement speed is 1 mm s^{-1} , the kinetic energy of the tip-ball obtained is $1 \times 10^{-9}\text{J}$. The depleted elastic potential energy at every bounce can also be calculated by the Hertz theory [22], which is about $(1/6) \times 10^{-9}\text{J}$. Therefore, the necessary bouncing times are only six before the ball reaches a steady-state condition. In other words, as long as the natural frequency of our probe reaches 60 Hz, the signals of the probe will be stable in 0.1 s after contact.

The vibration modes of the probe have also been analyzed by the finite element method using ANSYS V12 software. The natural frequencies of different modes of the probe in vertical and rotational directions are listed in table 2. The natural frequencies of the first mode in vertical and rotational directions are 178 Hz and 340 Hz, respectively. Both are higher than the supplied electricity of 60 Hz and possible bouncing frequency of the mechanical probe. Figure 7 shows the fourth mode in vertical direction of the probe. We can find that the natural frequency of the fourth mode is 2548 Hz on the leaf springs. The floating plate and the stylus are comparatively more stable. The latter can also confirm the assumption of the rigid body motion of the floating plate in theoretical analysis.

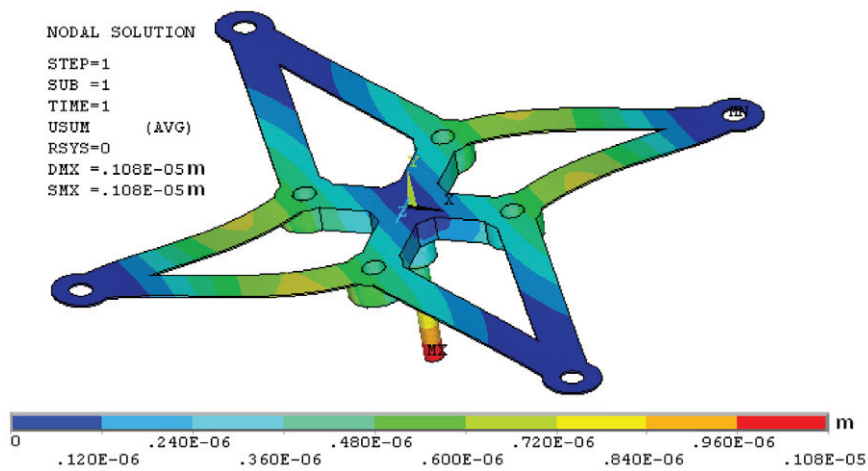
4. Experiments

4.1. Resolution

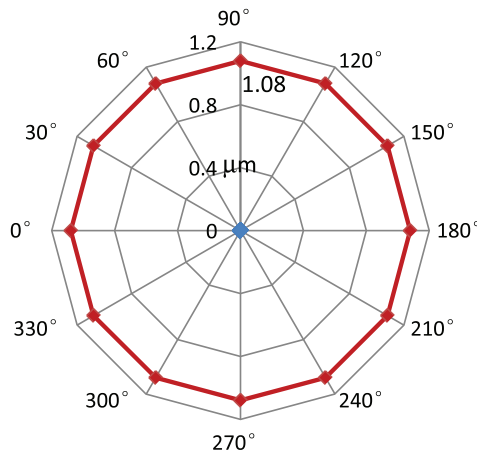
The signal-to-noise ratio (SNR) of the sensors' output signals determines the probe's resolution. For the two sine wave



(a) In vertical direction when the force is applied in Z direction



(b) In horizontal direction when the force is applied at 45° in XY plane



(c) Displacement distribution along different horizontal directions under 1mN force

Figure 6. The tip's displacement when a contacting force of 1 mN is applied.

Table 2. The natural frequency of the probe, in Hz.

Mode	1st	2nd	3rd	4th	5th
Vertical modes	178	474	476	2458	2508
Rotational modes	340	874	875	4707	4799

signals output from the Michelson interferometer, their signal magnitudes are more than 6.3 V (figure 8). With the technique of correcting the Heydemann errors developed by the authors' group [36], the out-of-orthogonality of two sinusoidal signals due to the polarization of the emitted light was corrected. Good Lissajous circles were achieved during the Z motion of

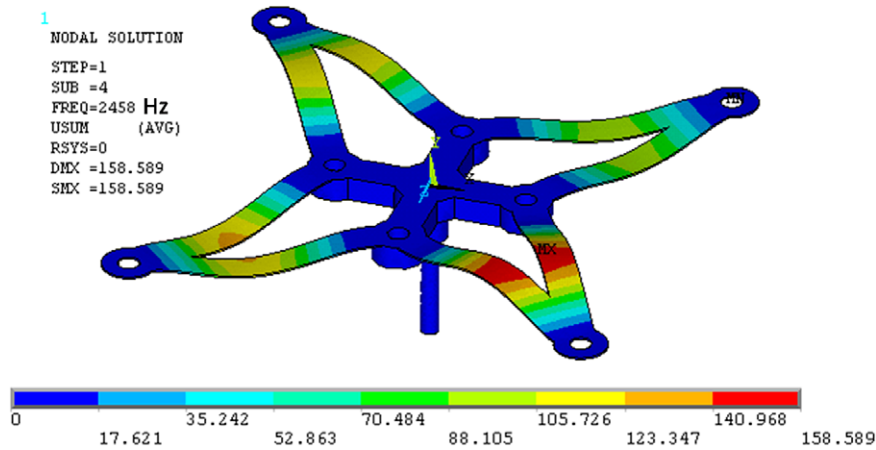


Figure 7. The fourth order natural frequency of the probe.

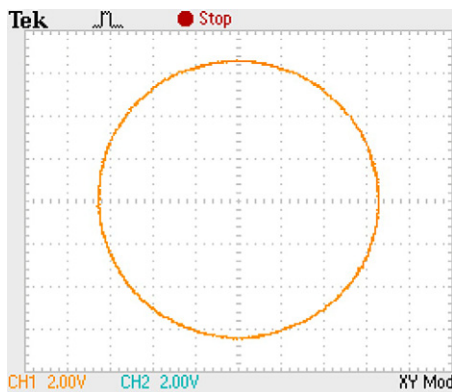


Figure 8. The normalized waveforms of the Michelson interferometer.

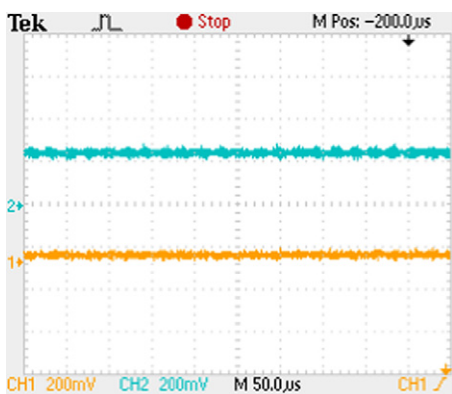


Figure 9. The noise level of the orthogonal signals.

the probe. The non-linearity error was 11 nm over the 20 μm range. Figure 9 shows the detected sine and cosine signals. The noise levels are both less than 70 mV. The wavelength of the adopted laser diode is 632.8 nm. Based on the principle of interferometer, one signal period corresponds to one-half wavelength. The phase subdivision could be done to one degree. Thus, the resolution of the Michelson interferometer can reach 0.9 nm.

Regarding the miniature autocollimator, the signal value corresponding to 10 μm measurement range is about 5.5 V, as shown in figure 10. In proportion, the required voltage

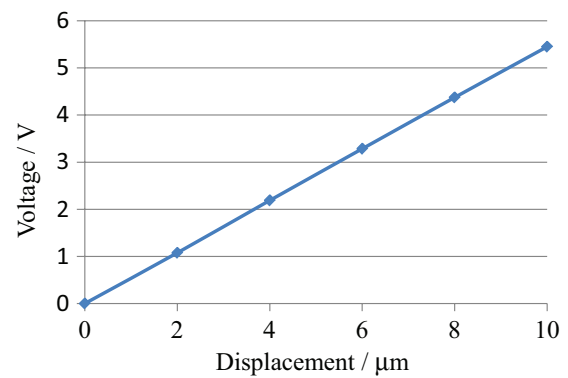


Figure 10. The measurement range in X+ direction.

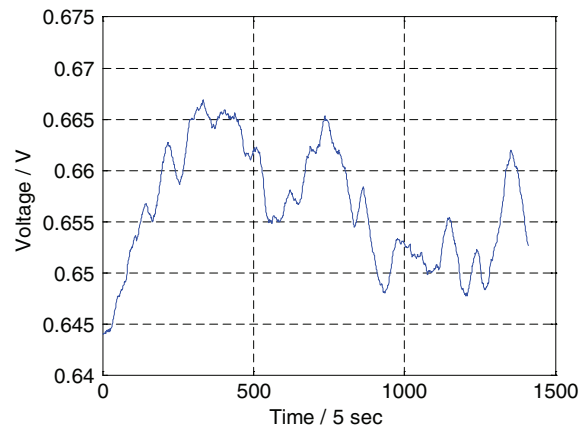


Figure 11. The noise level of the micro autocollimator.

resolution of 1 nm is 0.55 mV. After line fitting, the non-linearity error is less than 10 nm. Figure 11 shows one of the sensor's output signal processed by a hardware filter and a moving average program. Its noise level is less than 0.3 mV. Therefore, the probe can accomplish 1 nm resolution in the horizontal plane.

4.2. Stability

Several factors are probable to affect the stability of the probe, such as temperature, vibration, electromagnetic interference,

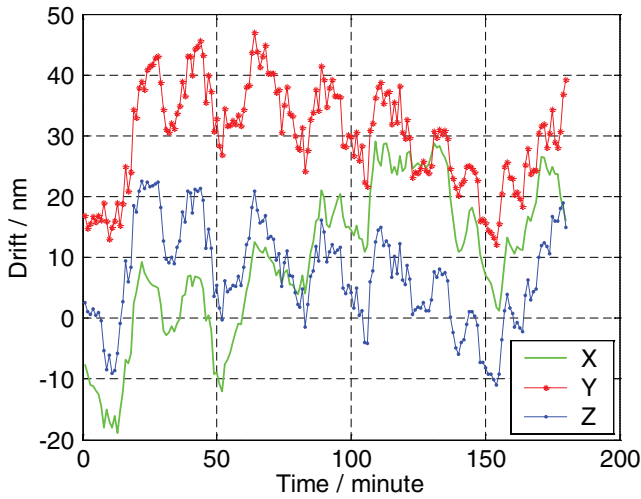


Figure 12. The results of the probe in a constant temperature chamber.

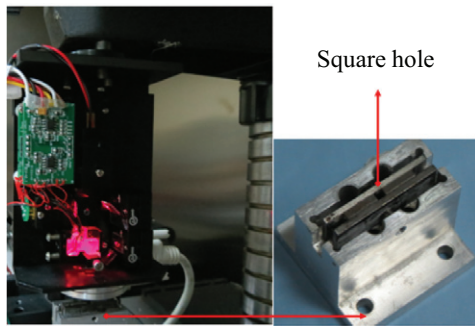


Figure 13. Photo of the experiment setup.

electrostatic interference, power supply and so on. Among these, the fluctuation of the environment temperature is deemed the primary factor. Although the temperature influence yields to the signal drifts of the circuit, the laser diode, the optical components and the QPD in the probe, the drifts are very small. The mechanical components and structure of the probe are much more sensitive to the temperature influence than the optical and electronic components [37].

In order to investigate the stability of the probe, an experiment of putting the probe in a constant temperature chamber was carried out. Acquiring the probe's output signals after the temperature in the chamber was stable (the temperature fluctuation range is less than 0.05 °C), the results are shown in figure 12. It is seen that the total drift of every coordinate axis was less than 50 nm for the duration of three hours. So the stability of the probe was confirmed.

4.3. Scanning range

In order to calibrate and test the probe, an experiment setup has been conducted. As shown in figure 13, the analogue contact probe is assembled in the frame of a stand. On the tested surface, a 2 mm × 2 mm square hole was formed by four high accuracy gauge blocks (right photo in figure 13) so as to contact the tip-ball from different horizontal directions.

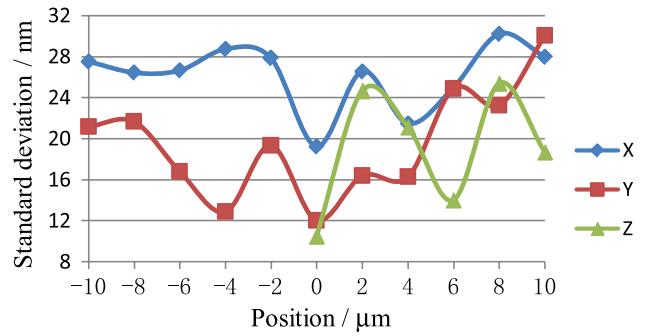


Figure 14. Measurement range and standard deviation.

The diameter of the tip-ball is 1 mm. The gauge blocks and the clamp were fixed onto a high precision 3D nano-positioning stage made by Physik Instrumente (PI, model P-611 with repeatability less than 25 nm and 100 μm × 100 μm travel) for the probe calibration in X and Y directions. For Z direction calibration, the P-753 model with repeatability less than 2 nm and 10 μm travel was adopted. The voltage signals from the 3D optical sensor are recorded via a DAQ card (PCI-6251, National Instruments).

Due to the fact that the probe's coordinate system cannot coincide with the 3D stage's coordinate system during installation, the probe coordinate system has to be measured and transformed through a matrix to the stage coordinate system before calibration. The stage's motion is taken as the reference with an interval of 2 μm. The probe's output signals (u, v, z) are recorded simultaneously. Thus, we can calculate the matrix coefficients by multiple linear regression method as expressed by equation (3).

$$\begin{bmatrix} X \\ Y \\ Z \end{bmatrix}^T = \begin{bmatrix} u \\ v \\ z \\ 1 \end{bmatrix}^T \begin{bmatrix} -2.4519 & 3.7012 & 0.40845 \\ -2.3657 & 3.3328 & 0.98048 \\ 0.0025172 & 0.00050569 & 0.0010522 \\ -0.35526 & 0.15103 & 0.6882 \end{bmatrix}. \quad (3)$$

Ten positions in X, Y directions and five positions in Z direction were repeatedly measured and the interval was 2 μm. The measurement procedure is the same in every direction. The first step is to let the probe ball enter the square hole by moving the stages. The second step is to move the block module and contact the probe by the 'double trigger method' [38]. The third step is to push the probe by a 10 μm displacement and record the probe's three output displacements—X, Y and Z. The fourth step is to move the stage back 10 μm and record the probe's three output displacements. Then repeat the forward and backward measurement six times and calculate the standard deviation in each axis. The results of these experiments are shown in figure 14. The measurement ranges were ±10 μm × ±10 μm × 10 μm (X × Y × Z) and the standard deviation was less than 30 nm in all directions.

5. Measurement examples

The probe has been installed in a micro-CMM developed by our group [1, 39]. Probing a sphere can reveal many errors of a 3D probing system. Unfortunately, a full 3D probing

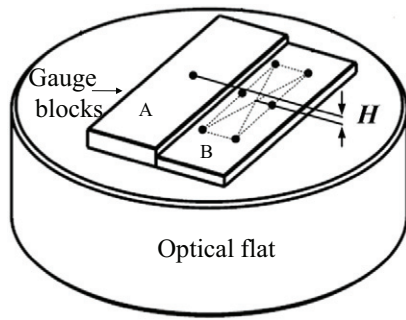


Figure 15. Optical flat and gauge blocks.

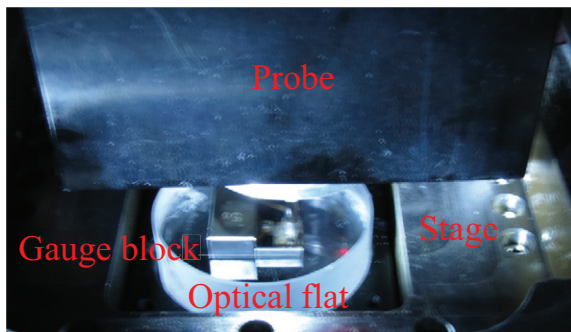


Figure 16. Picture of the gauge blocks under measurement.

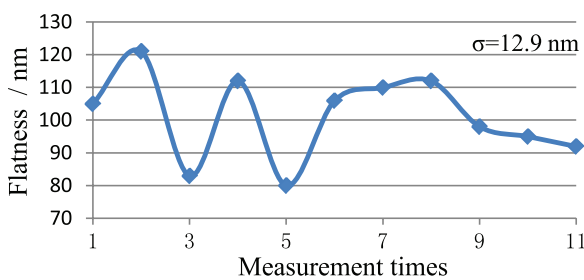


Figure 17. The results of the flatness measurement.

acceptance test on a sphere along the ISO 10360-2 norm could not be performed with the motion controller that we have today. Therefore, only flatness and step height measurement were conducted. Two grade 0 gauge blocks, named A and B, were put together on an optical flat, as shown in figure 15. The thickness of A is 5 mm and B is 2 mm. A picture of the gauge blocks under measurement is given in figure 16. The flatness of block B was measured 11 times, each time six uniformly distributed points were measured, as marked in figure 15. Fitting measured data with least-squares plane equation, the residual of each measured point was obtained. The peak-to-valley of the errors is evaluated as flatness error of the measured surface. Figure 17 shows the variation of flatness errors of 11 times. The average flatness is about 100nm and the standard deviation is 12.9 nm. When measuring the step height formed by blocks A and B, the center plane equation of block B was first obtained in the same way as the flatness measurement, and then the micro-CMM stage moved to probe the center point of block A. The distance from the point on block A to the center plane of block B was calculated. The step height was measured six times and the results are shown in figure 18.

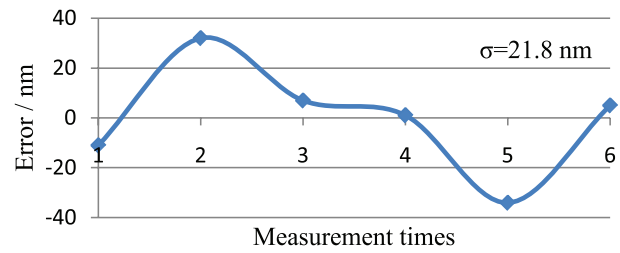


Figure 18. The measurement error of the step height.

The mean value of the step height is 2.999946mm and the standard deviation is 21.8 nm.

6. Conclusions

This paper has presented a new analogue contact probe for micro-CMM based on an elastic mechanism and a 3D optical sensor. The probe has been designed, simulated, manufactured, assembled and calibrated. Experimental results show that the probe can achieve equal stiffness (within $1 \text{ mN} \mu\text{m}^{-1}$), more than 178 Hz natural frequency, $\pm 10 \mu\text{m} \times \pm 10 \mu\text{m} \times 10 \mu\text{m}$ ($X \times Y \times Z$) measurement range and 30 nm measurement standard deviation. It meets the requirements for microstructure measurement.

Acknowledgement

The work reported is part of a research program funded by the State Key Laboratory of Precision Measuring Technology and Instruments of China, the National Natural Science Foundation of China, the National High Technology Research and Development Program of China (Grant No. 2008AA042409) and the Natural Science Foundation of Anhui Province for Higher Education Institutions (Grant No. KJ2014A021).

References

- [1] Fan K C, Fei Y T, Yu X F, Chen Y J, Wang W L, Chen F and Liu Y S 2006 Development of a low-cost micro-CMM for 3D micro and nano-measurements *Meas. Sci. Technol.* **17** 524–32
- [2] Dai G L, Bütetfisch S, Pohlenz F and Danzebrink H U 2009 A high precision micro/nano CMM using piezoresistive tactile probes *Meas. Sci. Technol.* **20** 084001
- [3] Jäger G, Manske E and Hausotte T, 2001 Nano-positioning and measuring machine *Proc. 2nd EUSPEN (Turin, May 2001)* vol 1 pp 290–3
- [4] Takamasu K, Furutani K R and Ozono S 1997 Development of nano-CMM (coordinate measuring machine) with nanometer resolution *Proc. XIV IMEKO World Congress (Finland, June 1997)* vol 8 pp 34–9
- [5] Hughes E B, Wilson A and Peggs G N 2000 Design of high accuracy CMM based on multi-lateration techniques *Ann. CIRP* **49** 391–4
- [6] Leach R K and Murphy J 2004 The design of co-ordinate measuring probe for characterizing truly three-dimensional micro-structures *4th EUSPEN Int. Conf. (Glasgow, May–June 2004)* pp 230–1
- [7] Peggs G N, Lewis A J and Oldfield S 1999 Design for a compact high-accuracy CMM *Ann. CIRP* **48** 417–20

- [8] Tan J B and Cui J N 2010 Ultraprecision 3D probing system based on spherical capacitive plate *Sensors Actuators A* **159** 1–6
- [9] Haitjema H, Pril W O and Schellekens P 2001 Development of a silicon-based nanoprobe system for 3D measurements *Ann. CIRP* **50** 365–8
- [10] Peiner E, Balke M, Doering L and Brand U 2008 Tactile probes for dimensional metrology with microcomponents at nanometre resolution *Meas. Sci. Technol.* **19** 064001
- [11] Tibrewala A, Phataralaoha A and Büttgenbach S 2009 Development, fabrication and characterization of a 3D tactile sensor *J. Micromech. Microeng.* **19** 125005
- [12] Guo H X and Fujita D 2011 Developments of scanning probe microscopy with stress/strain fields *Rev. Sci. Instrum.* **82** 123706
- [13] Küng A, Meli F and Thalmann R 2007 Ultraprecision micro-CMM using a low force 3D touch probe *Meas. Sci. Technol.* **18** 319–27
- [14] Hughes E B, Wilson A and Peggs G N 2000 Design of high accuracy CMM based on multilateration techniques *Ann. CIRP* **49** 391–4
- [15] Muralikrishnan B, Stone J A and Stoup J R 2006 Fiber deflection probe for small hole metrology *Precis. Eng.* **30** 154–64
- [16] Kim S W 2001 New design of precision CMM based upon volumetric phase-measuring interferometry *Ann. CIRP* **50** 357–60
- [17] Ji H, Hsu H Y, Kong L X and Wedding A B 2009 Development of a contact probe incorporating a Bragg grating strain sensor for nano coordinate measuring machines *Meas. Sci. Technol.* **20** 095304
- [18] Ding B Z, Fei Y T and Fan Z G 2009 3D touch trigger probe based on fiber Bragg gratings *Proc. SPIE* **7272** 72722U
- [19] Liu F F, Fei Y T, Xia H J and Chen L J 2012 A new micro/nano displacement measurement method based on a double-fiber Bragg grating (FBG) sensing structure *Meas. Sci. Technol.* **23** 054002
- [20] Enami K, Kuo C C, Nogami T, Hiraki M, Takamasu K and Ozono S 1999 Development of nano-probe system using optical sensing *IMEKO-XV World Congress (Osaka, June 1999)* pp 189–92
- [21] Fan K C, Cheng F, Wang W L, Chen Y J and Lin J Y 2010 A scanning contact probe for a micro-coordinate measuring machine (CMM) *Meas. Sci. Technol.* **21** 054002
- [22] Chu C L and Chiu C Y 2007 Development of a low-cost nanoscale touch trigger probe based on two commercial DVD pick-up heads *Meas. Sci. Technol.* **18** 1831–42
- [23] Liebrich T and Knapp W 2010 New concept of a 3D-probing system for micro-components *CIRP Ann. Manuf. Technol.* **59** 513–6
- [24] Panasonic Company 2013 UA3P-300/4/5 <http://industrial.panasonic.com>
- [25] Balzer F G, Hausotte T, Dorozhovets N, Manske E and Jager G 2011 Tactile 3D microprobe system with exchangeable styli *Meas. Sci. Technol.* **22** 094018
- [26] Michihata M, Takaya Y and Hayashi T 2008 Nano position sensing based on laser trapping technique for flat surfaces *Meas. Sci. Technol.* **19** 084013
- [27] Kim B, Masuzawa T and Bourina T 1999 The vibroscanning method for the measurement of micro-hole profiles *Measurement* **10** 697–705
- [28] Claverley J D and Leach R K 2010 A vibrating micro-scale CMM probe for measuring high aspect ratio structures *Microsyst. Technol.* **16** 1507–12
- [29] Hidaka K, Danzebrink H U, Illers H, Saito A and Ishikawa N 2010 A high-resolution, self-sensing and self-actuated probe for micro-and nano-coordinate metrology and scanning force microscopy *CIRP Ann. Manuf. Technol.* **59** 517–20
- [30] Weckenmann A, Peggs G and Hoffmann J 2006 Probing systems for dimensional micro and nano-metrology *Meas. Sci. Technol.* **17** 504–9
- [31] Bos E J C 2011 Aspects of tactile probing on the micro scale *Precis. Eng.* **35** 228–40
- [32] Li R J, Fan K C, Tao S, Qian J Z, Huang Q X and Cheng F 2011 Design of an analogue contact probe for nano-coordinate measurement machines (CMM) *Proc. SPIE* **8321** 832114
- [33] Li R J, Fan K C, Huang Q X, Qian J Z, Gong W and Wang Z W 2012 Design of a large scanning range contact probe for nano-coordinate measurement machines (CMM) *Opt. Eng.* **51** 081503
- [34] Li R J, Fan K C, Zhou H, Wang N and Huang Q X 2013 Elastic mechanism design of the CMM contact probe *Proc. SPIE* **8916** 89160P
- [35] Büchner H J and Jäger G 2006 A novel plane mirror interferometer without using corner cube reflectors *Meas. Sci. Technol.* **17** 746–52
- [36] Wu X L, Zhang H, Tseng Y Y and Fan K C 2013 A robust sinusoidal signal processing method for interferometers *Proc. SPIE* **8916** 89160N
- [37] Li R J, Fan K C, Qian J Z, Huang Q X, Gong W and Miao J W 2012 Stability analysis of a contact scanning probe for micro/nano-CMM *Nanotechnol. Precis. Eng.* **10** 125–31
- [38] Cheng F, Fan K C and Fei Y T 2010 Measurement of pre-travel distance of a touch probe for nano-CMM *Nanotechnol. Precis. Eng.* **8** 107–13
- [39] Fan K C, Cheng F, Wang H Y and Ye J K 2012 The system and the mechatronics of a pagoda type micro-CMM *Int. J. Nanomanuf.* **8** 67–86